Two-dimensional quantum turbulence in a nonuniform Bose-Einstein condensate

T.-L. Horng,[1] C.-H. Hsueh,[2] S.-W. Su,[3] Y.-M. Kao,[2] and S.-C. Gou[2]

[1]*Department of Applied Mathematics, Feng Chia University, Taichung 40724, Taiwan*
[2]*Department of Physics, National Changhua University of Education, Changhua 50058, Taiwan*
[3]*Department of Physics, National Tsing Hua University, Hsinchu 30047, Taiwan*
(Received 26 May 2009; published 24 August 2009)

We investigate the dynamics of turbulent flow in a two-dimensional trapped Bose-Einstein condensate by solving the Gross-Pitaevskii equation numerically. The development of the quantum turbulence is activated by the disruption of an initially embedded vortex quadrupole. By calculating the incompressible kinetic-energy spectrum of the superflow, we conclude that this quantum turbulent state is characterized by the Kolmogorov-Saffman scaling law in the wave-number space. Our study predicts the coexistence of two subinertial ranges responsible for the energy cascade and enstrophy cascade in this prototype of two-dimensional quantum turbulence.

I. INTRODUCTION

The turbulent flow in superfluid is an important and long-standing subject in low-temperature physics [1]. It was already known in the early 1950s that the flow of superfluid component of liquid helium can become turbulent in the presence of a counterflow of the two fluids driven by a steady-injected heat current [1]. Feynman speculated that this superfluid turbulence can be described as a chaotic tangle of quantized vortex filaments [2]. Later, Vinen experimentally confirmed this picture by showing that superfluid turbulence is maintained by the mutual friction between vortices and the normal flow [3]. Subsequently, superfluid turbulence in the thermal counterflow was intensively investigated and many aspects of this type of turbulence are now well understood. Nevertheless, due to the complexity of the two-fluid structure, the counterflow turbulence has no classical analog and thus attracted little attention of the investigators working on classical hydrodynamics. More recently, superfluid turbulence of noncounterflow types have been achieved experimentally in liquid helium, in analogy with some rather simple cases of classical turbulence (CT). For example, Maurer and Tabeling demonstrated the generation of turbulence by two counter-rotating disks [4] and Stalp *et al.* observed the decay of grid turbulence [5].

Superfluid turbulence is sometimes termed as quantum turbulence (QT) to highlight the key role played by quantized vortices in the dynamics which differs from that of the chaotic but continuous vorticity of CT. Despite the fundamental difference between QT and CT, experimental evidences [4,5] and numerical simulations [6–8] have revealed that, even at very low temperatures, QT is characterized by an energy spectrum following the Kolmogorov's −5/3 power law, a sign that also hallmarks the occurrence of CT [9]. These findings have aroused considerable interest in exploring the possible connection between CT and QT occurring at zero temperature. In particular, due to the close relationship between liquid helium and atomic Bose-Einstein condensate (BEC) in superfluid behavior and quantized vorticity [10], QT in the trapped BEC has been well studied by several groups in the last few years. In these investigations, QT is predicted to occur in the following cases: in the evolving stage prior to the nucleation of vortex lattice in a rotating condensate [11,12], in the collision of two condensates [13], in the combined rotations around different axes of a condensate [14], in the disruption of a single vortex ring through bending wave instability [15], and in a phase-imprinted two-dimensional (2D) BEC [16].

From the perspective of classical statistical physics, the fully developed turbulence can be explained by means of the transport of inviscid invariants between different scales. With this reasoning, Kolmogorov assumed that CT is statistically self-similar in an inertial range of wave number k, where energy can be transferred from large scales to small scales at a constant rate ϵ without being dissipated by viscosity, a process called cascade [9]. Using simple dimensional analysis, Kolmogorov obtained a scaling law for the energy spectrum $\mathcal{E}(k) \sim \epsilon^{2/3} k^{-5/3}$, which imposes a general criterion for characterizing three-dimensional (3D) CT. Here the energy spectrum $\mathcal{E}(k)$ is defined as $\mathcal{E} = \int dk \mathcal{E}(k)$, where $\mathcal{E}$ is the total incompressible kinetic energy and $\epsilon = d\mathcal{E}/dt$. Kraichnan [17] and Batchelor [18] (hereafter referred to as KB) extended Kolmogorov's theory to 2D turbulence by considering enstrophy (half of the integral of squared vorticity) as a second inviscid invariant. According to KB theory, the dual cascades of energy and enstrophy give rise to two distinct scaling regimes for 2D turbulence in the inviscid limit. For forced 2D turbulence, specifically, where energy and enstrophy are injected into the flow at a given wave number k_f, enstrophy tends to cascade from k_f toward higher k, leading the energy spectrum to fall off like k^{-3} in this regime. On the other hand, energy tends to cascade upward, i.e., from k_f toward lower k, with the kinetic-energy spectrum scaling like $k^{-5/3}$, which is also known as the inverse cascade. As for the decaying 2D turbulence, KB theory also predicts a k^{-3} spectrum in the inertial range. More detailed review of the theory and phenomenology of 2D CT can be found in Ref. [19] and all references therein.

Although the picture of enstrophy cascade proposed by KB theory is also supported by other approaches, such as the closure theory and closure calculations, however, direct numerical simulations do not very strongly support the k^{-3} law [19]. In fact, depending on the numerical schemes employed,

the power law of the energy spectrum in the enstrophy cascade regime appears in divergent disagreements with k^{-3} law [19], leaving 2D CT open to question. For all that, it is still significant to ask whether there exists any analog between 2D CT and QT just as the Kolmogorov's $-5/3$ power law being common in the 3D cases for CT and QT. In this work, we study the turbulent dynamics of the 2D BEC confined in a harmonic trap $V(\boldsymbol{\rho}) = (1/2)m\omega^2(x^2 + \lambda_y^2 y^2)$ by numerically solving the time-dependent GP equation. We shall carry out the computations in the oscillator units for mathematical convenience, in which the length, time, and energy are, respectively, scaled in units of $(\hbar/m\omega)^{1/2}$, ω^{-1} and $\hbar\omega$, and the time-dependent GP equation takes the following dimensionless form:

$$i\frac{\partial\Psi(\boldsymbol{\rho},t)}{\partial t} = \left(-\frac{\nabla^2}{2} + \frac{x^2 + \lambda_y^2 y^2}{2} + g|\Psi(\boldsymbol{\rho},t)|^2\right)\Psi(\boldsymbol{\rho},t). \quad (1)$$

Here, $\boldsymbol{\rho} = (x,y)$ and the condensate wave function $\Psi(\boldsymbol{\rho},t)$ is normalized by $\int|\Psi(\boldsymbol{\rho},t)|^2 d\boldsymbol{\rho} = 1$. Correspondingly, the coupling strength is expressed by $g = 4\pi\tilde{a}N$, where N is the total number of atoms in the condensate and $\tilde{a}$ is the effective s-wave scattering length in 2D space.

The organization of this paper is as follows. In Sec. II, the time evolution of the wave function $\Psi(\boldsymbol{\rho},t)$ is solved by numerically integrating Eq. (1). Hydrodynamic properties that are relevant in examining the occurrence of turbulent flow in superfluid BEC, such as the kinetic energy, enstrophy are determined from the condensate wave function. In Sec. III, we discuss the scaling laws for the incompressible kinetic-energy spectrum. In particular, a scenario for dual cascade in 2D trapped BEC is presented. Finally, some concluding remarks are given in Sec. IV.

II. NUMERICAL INTEGRATIONS OF THE GROSS-PITAEVSKII EQUATION

To numerically integrate Eq. (1), we use the method of lines with spatial discretization by highly accurate Fourier pseudospectral method and time integration by adaptive Runge-Kutta method of orders 2 and 3 (RK23). Furthermore, to stir the condensate to turbulence, we assume that a vortex quadrupole consisting of two singly quantized vortices located at $(\pm4, 0)$ and two singly quantized antivortices located at $(0, \pm4)$ is initially placed in an isotropic condensate $(\lambda_y = 1)$ with a Thomas-Fermi (TF) radius $R_{TF} = \sqrt{2\mu} = 6$, where μ is the chemical potential of the condensate. Such a configuration can be constructed following the method described in Ref. [20]. The time evolution of the above vortex configuration is shown in Fig. 1 by plotting $|\Psi(\boldsymbol{\rho},t)|^2$ at various times. In Figs. 1(b)–1(d), we see that the vortices first pair up as two vortex dipoles under the influence of trap potential [Fig. 1(b)] and start to traverse in the condensate. Since vortex is a phase singularity and can rotate the mass surrounding it, the traveling vortices that pass through the outer dilute area of the trapped BEC can generate surface waves. Consequently, the interplay between surface waves creates mass blobs of opposite phases in the outer dilute area, which may collide with each other and nucleate vortices via
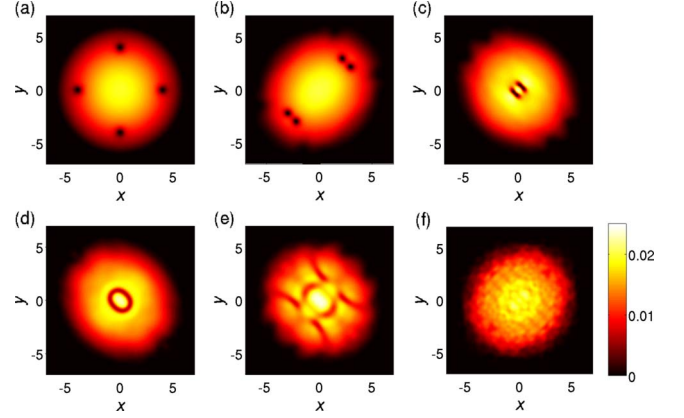

FIG. 1. (Color online) Density profile of the trapped BEC at various times: (a) $t=0$, two singly quantized vortices and two singly quantized antivortices are located at $(\pm4, 0)$ and $(0, \pm4)$, respectively, in a condensate with $R_{TF}=6$ and $\lambda=1$; (b) $t=3.5$; (c) $t=5.4$, annihilation of the four energetic vortices in the central region; (d) $t=5.8$, an outwardly propagating shock wave is formed; (e) $t=9.5$; and (f) $t=100$, achieving the stationary turbulent state.

snake instability. Now as time goes on, the two vortex dipoles move toward each other along the line $y=x$ under mutual interaction and eventually come to a head-on collision, which annihilates all initial vortices and forms a radially expanding ringlike dark soliton preceded by a shock wave. Owing to the trapping potential, the outgoing shock wave is reflected at the border area and subsequently pulsates in the condensate for a while. This back-and-forth pulsation gives rise to more violent surface waves which would also generate vortices as described above. Apart from the above mechanism, the shock wave itself could also generate vortices when traveling in the outer dilute area. Such a mechanism is discussed by Hau in Ref. [21], where the shock wave causes stripes of dark or gray soliton (vortex sheet), which evolves later into vortices via snake instability.

The pulsation of the shock wave fades until most of its energy disperses and causes significant density fluctuations inside the condensate. After this stage, the sound waves (density fluctuations) fully develop in the interior of the condensate, whereas all newly generated quantized vortices are driven to the outer region of the condensate. Finally, after a sufficiently long period, say $t=100$, the density profile of the condensate is plotted in Fig. 1(f), where the cumuluslike pattern of the spatial distribution suggests that the superflow might have become turbulent there.

In applying the spectral scaling approach to identify the occurrence of turbulence in the trapped BEC, it is more appropriate to express the condensate wave function in the form of Madelung transformation, namely, $\Psi(\boldsymbol{\rho},t) = \sqrt{n(\boldsymbol{\rho},t)}\exp[i\varphi(\boldsymbol{\rho},t)]$. Substituting the above form into Eq. (1), we obtain the continuity equation and Euler equation, respectively,

$$\frac{\partial}{\partial t}n + \nabla \cdot (n\mathbf{u}) = 0, \quad (2)$$

$$\frac{\partial}{\partial t}\mathbf{u} + \mathbf{u} \cdot \nabla \mathbf{u} = -\nabla Q, \qquad (3)$$

where $\mathbf{u}(\boldsymbol{\rho},t) = \nabla \varphi(\boldsymbol{\rho},t)$ is the velocity field of the superflow and $Q = gn + V - (\nabla^2 \sqrt{n})/2\sqrt{n}$. The total-energy functional is calculated in terms of n and $\mathbf{u}$, that can be expressed as the sum of four terms

$$E_{tot} = \int \left(\frac{1}{2}|\nabla \sqrt{n}e^{-i\varphi}|^2 + \frac{x^2 + \lambda_y^2 y^2}{2}n + \frac{1}{2}gn^2 \right) d\boldsymbol{\rho}$$
$$= E_{kin} + E_q + E_{tr} + E_{int}, \qquad (4)$$

where

$$E_{kin} = \frac{1}{2}\int |\sqrt{n}\mathbf{u}|^2 d\boldsymbol{\rho},$$

$$E_q = \frac{1}{2}\int (\nabla \sqrt{n})^2 d\boldsymbol{\rho},$$

$$E_{tr} = \frac{1}{2}\int n(x^2 + \lambda_y^2 y^2)d\boldsymbol{\rho},$$

$$E_{int} = \frac{1}{2}\int gn^2 d\boldsymbol{\rho},$$

represent the superfluid kinetic energy, the quantum pressure energy, the trap energy, and the interaction energy, respectively. Following Ref. [7], we decompose the vector field $\sqrt{n}\mathbf{u}$ into the solenoidal and irrotational parts or, correspondingly, the incompressible and compressible parts, i.e., $\sqrt{n}\mathbf{u} = (\sqrt{n}\mathbf{u})^i + (\sqrt{n}\mathbf{u})^c$, where $\nabla \cdot (\sqrt{n}\mathbf{u})^i = 0$ and $\nabla \times (\sqrt{n}\mathbf{u})^c = 0$. To accomplish such decomposition, we may let $(\sqrt{n}\mathbf{u})^i = \nabla \times \mathbf{A}$ and $(\sqrt{n}\mathbf{u})^c = \nabla \Theta$, where $\mathbf{A}$ and Θ are the vector and scalar potentials for the field $\sqrt{n}\mathbf{u}$, such that $\sqrt{n}\mathbf{u} = \nabla \times \mathbf{A} + \nabla \Theta$. Taking divergence on both sides of the last expression, we get the Poisson equation for the scalar potential

$$\nabla^2 \Theta = \nabla \cdot (\sqrt{n}\mathbf{u}), \qquad (5)$$

which can be numerically solved by Fourier pseudospectral method. Once the scalar potential Θ is numerically solved, the vector potential $\mathbf{A}$ can be determined and, hence, the field components $(\sqrt{n}\mathbf{u})^i$ and $(\sqrt{n}\mathbf{u})^c$. Thus, the incompressible and compressible kinetic energies are defined by $E_{kin}^{i,c} = (1/2)\int d\boldsymbol{\rho}|(\sqrt{n}\mathbf{u})^{i,c}|^2$. Moreover, since $(\sqrt{n}\mathbf{u})^i$ and $(\sqrt{n}\mathbf{u})^c$ are mutually orthogonal, it follows that $E_{kin} = E_{kin}^i + E_{kin}^c$. Physically, E_{kin}^i and E_{kin}^c correspond to the kinetic energies of swirls and sound waves in the superflow, respectively. Apart from the kinetic energy, we also need to calculate the enstrophy of the superflow for comparison with the results of 2D CT. Classically, the enstrophy Z is defined by $Z = (1/2)\int |\boldsymbol{\omega}|^2 d\boldsymbol{\rho}$, where $\boldsymbol{\omega}$ is the vorticity vector. In this paper, in analogy with the replacement $\mathbf{u} \rightarrow \sqrt{n}\mathbf{u}$, for nonuniform condensate density, we use the modified vorticity vector,
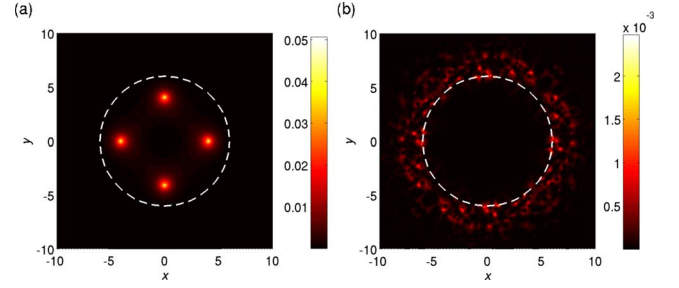

FIG. 2. (Color online) Spatial distribution of the incompressible kinetic energy E_{kin}^i at (a) $t=0$; (b) $t=100$. The circle of white dashed line indicates the Thomas-Fermi radius of the condensate ($R_{TF}=6$).

$$\boldsymbol{\omega} = \nabla \times (\sqrt{n}\mathbf{u}) = \nabla \sqrt{n} \times \mathbf{u} + \sum_j 2\pi s_j \sqrt{n}\delta(\boldsymbol{\rho} - \boldsymbol{\rho}_j)\hat{\mathbf{z}}, \quad (6)$$

instead of the usual form $\boldsymbol{\omega} = \nabla \times \mathbf{u}$ to evaluate the density of enstrophy in a trapped BEC. Here $2\pi s_j(s_j = \pm 1)$ is the circulation quantum carried by the jth vortex and the delta functions entering in the right-hand side indicate the locations of singularity of the enstrophy distribution. It should be clarified that, although Eq. (6) introduces anomalous generation of vorticity due to the gradient of density in addition to the usual contribution made by quantized vortices, the first term in the right-hand side of Eq. (6) only contribute slightly to the total vorticity as we shall see in the following demonstrations in Fig. 4. As a matter of fact, the definition of vorticity is not crucial for the current study since $\boldsymbol{\omega}$ is not involved in the calculations of kinetic-energy spectrum.

The profiles of $|(\sqrt{n}\mathbf{u})^{i,c}|^2/2$ and $|\boldsymbol{\omega}|^2/2$, at $t=0$ and 100 are shown separately in Figs. 2–4. Initially, E_{kin}^i and Z are compactly localized around the core of each individual quantized vortex whose singular nature is revealed by the granular distribution of Z. The snapshot of the spatial distributions for $E_{kin}^{i,c}$ and Z at a much later instant of time $t=100$ are shown in Figs. 2(b), 3(b), and 4(b) for comparison. We see that the incompressible field is almost distributed in the outer annular area of the condensate with $6 \lesssim |\boldsymbol{\rho}| \lesssim 8$, whereas the compressible field is largely distributed in the inner region with $|\boldsymbol{\rho}| \lesssim 6$. Thus, the incompressible and compressible components of the kinetic energy are basically spatially separated despite that they somewhat overlap around the border area about $|\boldsymbol{\rho}| \approx 6$. This result is consistent with the scenario of vortex-sound separation in our previous study for the for-
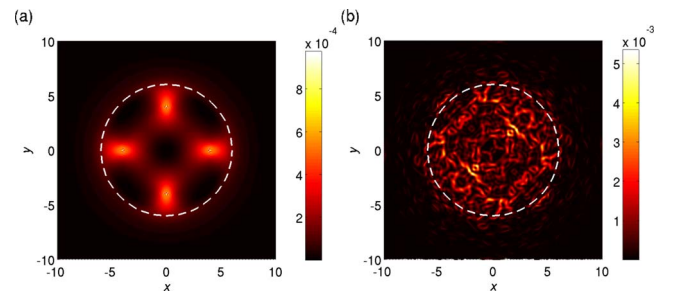

FIG. 3. (Color online) Spatial distribution of the compressible kinetic energy E_{kin}^c at (a) $t=0$; (b) $t=100$. The circle of white dashed line indicates the Thomas-Fermi radius of the condensate ($R_{TF}=6$).
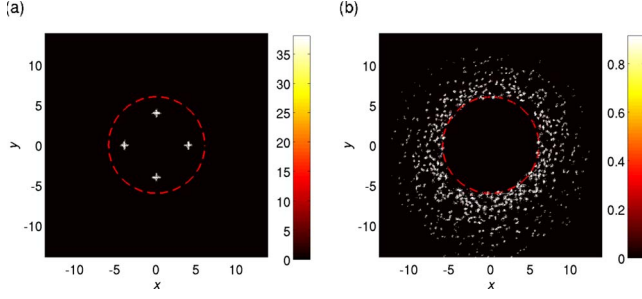
FIG. 4. (Color online) Spatial distribution of the enstrophy Z at (a) $t=0$; (b) $t=100$. The circle of red dashed line indicates the Thomas-Fermi radius of the condensate ($R_{TF}=6$). Comparing the present figures with Fig. 2, we see that the distribution of Z basically coincides with that of E_{kin}^i. Obviously, every brightest speck indicates the core of a quantized vortex. On the other hand, in the interior region of the condensate that is free from vortices, the distribution of vorticity is scarcely detectable, indicating that the contribution of the term $\nabla\sqrt{n}\times\mathbf{u}$ to the total enstrophy can be neglected.

mation of QT in a 3D BEC [15], and Fig. 4(b) indicates very clearly that all vortices are randomly localized in the outer region.

The time evolutions of kinetic energies and enstrophy in the time interval $0\leq t\leq 100$ are illustrated in Fig. 5. By virtue of the initial vortex configuration, E_k^c comes up at a much smaller value than E_k^i initially. However, the subsequent motion of the vortices causes E_k^c and Z to increase but E_k^i to decrease shortly after the evolution sets out. In particular, the movement of the vortices toward the high-density central region leads to a rapid rise in the enstrophy as shown in Fig. 5(b). Nevertheless, both E_{kin}^i and Z have an abrupt drop in the period $5.5\leq t\leq 6.0$, when the four initial vortices are driven to annihilate each other at the central region, which is consistent with our previous observation.

From Fig. 5, we see that E_{kin}^i and E_{kin}^c stay almost stationary when the system reaches fully turbulent, yet the fluctuations about their mean values reveal the occurrence of intensive energy interchange between all components of the total energy. To gain more insight into this observation, here we derive an equation which relates the change rate of E_{kin}^i to that of E_{kin}^c. In doing so, we first note that Eqs. (2) and (3)
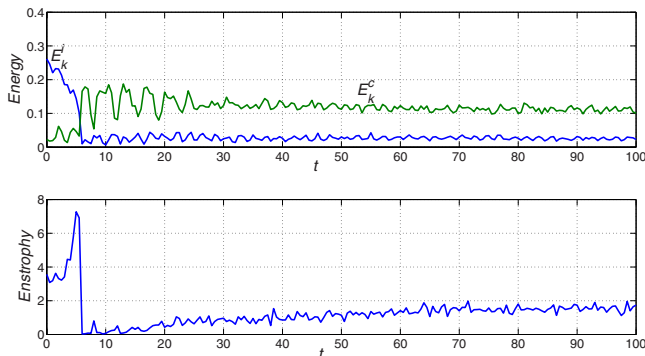

FIG. 5. (Color online) Time developments of the incompressible/compressible kinetic energy (upper) and the enstrophy (lower).

can be combined to yield the continuity equation for the current $\mathbf{J}=n\mathbf{u}$, i.e.,

$$\frac{\partial \mathbf{J}}{\partial t} + \nabla\cdot(\mathbf{J}\mathbf{u}) = -n\,\nabla Q. \tag{7}$$

Adding up the inner product of $\mathbf{u}$ and Eq. (7), together with that of $\mathbf{J}$ and Eq. (3), we obtain

$$\frac{1}{2}\frac{\partial}{\partial t}(n|\mathbf{u}|^2) = -\frac{1}{2}\nabla\cdot(\mathbf{J}|\mathbf{u}|^2) - \mathbf{J}\cdot\nabla Q. \tag{8}$$

Consequently, the change rate of the total kinetic energy can be obtained by taking volume integral over the whole space in both sides of the last equation and this leads to the following identity:

$$\frac{d}{dt}(E_{kin}^i + E_{kin}^c) = -\int \mathbf{J}\cdot\nabla Q d\boldsymbol{\rho}, \tag{9}$$

where the integral of the first term in the right-hand side of Eq. (8) vanishes as a consequence of Stokes theorem. Equation (9) then accounts for the balance of energy, in the sense that the change in the total kinetic energy is compensated by the work done by the field $-\nabla Q$ on the trapped condensate particles. Accordingly, the power in the right-hand side of Eq. (9) represents the sum of conversions of E_{int}, E_{tr}, and E_q, into the *total kinetic energy*. Note that it is not possible to figure out exactly the fractions of power converting, respectively, into E_{kin}^i and E_{kin}^c from further derivations of Eq. (9). However, from Fig. 5, we see that E_{kin}^i and E_{kin}^c do constantly fluctuate around their mean values, suggesting that energy interchange between incompressible and compressible fields mediated by the field $-\nabla Q$ occurs from time to time in the condensate. Now, since we consider the scaling behavior of the spectrum of E_{kin}^i as the sole criterion for identifying the formation of QT, it is expected that E_{kin}^c, which is inseparable from E_{kin}^i, may play a significant role in the dynamics of QT in the trapped BEC, and this will be addressed in the following section.

III. SCALING LAWS OF THE INCOMPRESSIBLE KINETIC-ENERGY SPECTRUM

The angle-averaged kinetic-energy spectrum $E_{kin}^{i,c}(k)$, as a function of wave number k, is defined by [7]

$$E_{kin}^{i,c}(k) = \frac{k}{2}\int d\phi |\mathcal{F}[(\sqrt{n}\mathbf{u})^{i,c}]|^2, \tag{10}$$

such that $E_{kin}^{i,c}=\int_0^\infty E_{kin}^{i,c}(k)dk$. Here $\mathcal{F}[\dots]$ denotes the Fourier transform of a given function or vector field in 2D space. In Eq. (10), the integral over the k shell in the momentum space is accomplished by numerically summing over the grid points with $(k_x^2+k_y^2)^{1/2}=k$, where k_x and k_y are the Cartesian components of the wave vector $\mathbf{k}$. In analogy with Eq. (10), the angle-averaged enstrophy spectrum is defined by $Z(k)=(k/2)\int d\phi|\mathcal{F}[\boldsymbol{\omega}]|^2$ such that the total enstrophy is given by the integral $Z=\int_0^\infty Z(k)dk$. From Eq. (6), it follows that $Z(k)=k^2 E_{kin}^i(k)$, which is well known in the classical fluid dynamics.
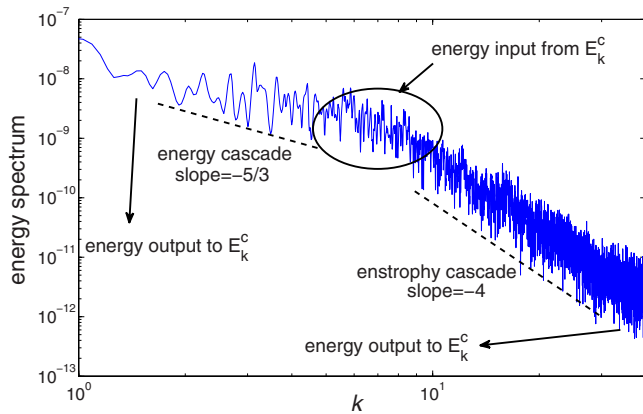
FIG. 6. (Color online) The incompressible kinetic-energy spectrum $E^i_{kin}(k)$ at $t=100$. This spectrum follows Kolmogorov's $k^{-5/3}$ law in the interval of $2<k<4$ and Saffman's k^{-4} law for $k>10$. The energy input regime is particularly marked with a circle.

With Eq. (10), we are now able to compute the spectra in question. In doing so, we have observed that although the velocity field of the superflow may change all the time, the energy spectrum $E^i_{kin}(k)$ evolves into a stationary form as time gets large. To be specific, let us consider the incompressible energy spectrum of the flow at $t=100$. Accordingly, we find that there are two ranges of spectral scaling, in which $E^i_{kin}(k)$ takes a power law as shown in Fig. 6. In the first range $2<k<4$, $E^i_{kin}(k)\sim k^{-5/3}$, which is consistent with the Kolmogorov spectrum and, in the second range $k>10$, $E^i_{kin}(k)$ follows closely with the k^{-4} law. Between these two ranges, there is a transitional zone $4<k<10$, where $E^i_{kin}(k)$ exhibits no scaling behavior. To double check the validity of the scaling laws, we calculate $Z(k)$ directly by numerical integration according to the definition for the angle-averaged spectrum. As expected, $Z(k)$ indeed exhibits the power-law behavior of $k^{-1/3}$ and k^{-2} correspondingly. Furthermore, to verify whether the spectral scaling behavior for $E^i_{kin}(k)$ depends on the geometry of the trapped BEC, we proceed to calculate $E^i_{kin}(k)$ for BEC with various values of R_{TF} and λ_y. Remarkably, all our numerical results indicate that when the quantum turbulent flow is well developed, only the $k^{-5/3}$ and k^{-4} ranges persist in $E^i_{kin}(k)$, whereas the k^{-3} spectrum as predicted by KB theory fails to develop in our system.

The emergence of $k^{-5/3}$ law in our numerical calculations for $E^i_{kin}(k)$ is well expected, as we have seen in various earlier studies concerning the turbulent motion of superflow in the 3D atomic condensate. In this work, we are more interested in the k^{-4} spectrum with QT in trapped BEC. As a matter of fact, the k^{-4} spectrum had been reported by some numerical calculations in 2D CT and Saffman conjectured that this scaling behavior is due to the dissipation of randomly distributed discontinuities of vorticity in the classical 2D turbulent flow [22]. In comparison with those classical cases, our results are consistent with Saffman's theory for the fact that there are indeed randomly distributed discontinuities of vorticity in the quantum turbulent flow as demonstrated in Fig. 4(b). On the other hand, the derivation of k^{-4} spectrum as a dissipation spectrum in Saffman's theory is inconsistent with our presumption on the nondissipative dynamics gov-
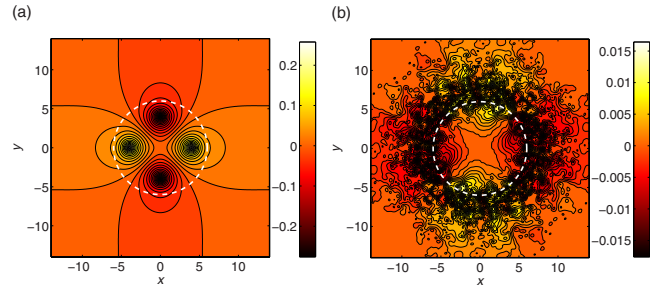

FIG. 7. (Color online) The streamlines or the level contours of the stream function $\phi(\boldsymbol{\rho})$ associated with the superflow at (a) $t=0$; (b) $t=100$. The circle of red dashed line indicates the Thomas-Fermi radius of the condensate ($R_{TF}=6$). The false colors indicate the values of $\phi(\boldsymbol{\rho})$.

erned by Eq. (1). Such a discrepancy might be explained in terms of energy transfer between E^i_{kin} and E^c_{kin} as we shall see in the following passages. Furthermore, we note that the spectrum shown in Fig. 5 shares some similarities with those of forcing 2D CT, although both dissipation and external forcing are not taken into account in the present problem. The coexistence of $k^{-5/3}$ and k^{-4} spectra draws forth the following question: does a quantum analog for dual cascades in 2D CT exist in the 2D turbulent superflow of a trapped BEC?

A straightforward way for probing into the above question is to evaluate the cascade rates of E^i_{kin} and the associated energy flux through the wave number k by solving the scale-by-scale energy budget equations derived from GP equation [23]. However, as we have shown in Fig. 1, the temporal and spatial variations in the modulus of the order parameter $\sqrt{n(\boldsymbol{\rho},t)}$ can no longer be ignored in the turbulent regime and, consequently, some extra terms mixing up the energy contents of two different kinematic categories (incompressible and compressible) would enter the desired equation. This makes the scale-by-scale calculations for the cascade rate and energy flux through wave number k for E^i_{kin} extremely complicated by using the method of Ref. [23]. Therefore, to circumvent this difficulty, we shall give an empirical interpretation of the cascading process in the current problem based on the numerical results so far presented. In doing so, let us survey some subtle ingredients of the model. The first subtlety is the meaning of the "size" for an energy-carrying eddy in a trapped BEC. From the definition of the vorticity vector $\boldsymbol{\omega}$ [Eq. (6)], we note that the singular and regular parts of $\boldsymbol{\omega}$ are modulated by $\sqrt{n}$ and its gradient, respectively. As a result, the magnitude of vorticity $|\boldsymbol{\omega}|$ of a vortex in high-density area is greater than that of a vortex in low-density area and, with such reasoning, we say that an eddy is energetically "larger" if it contains more circumfluent particles. In Fig. 7, the streamlines or the level curves of $\phi(\boldsymbol{\rho})=C$ for various values of the constant C are plotted for the flow at $t=0$ and $t=100$, respectively, where $\phi(\boldsymbol{\rho})$ is the stream function [24] associated with the velocity field and the false colors indicate the corresponding values of $\phi(\boldsymbol{\rho})$. To be conspicuous, part of Fig. 7(b) is enlarged and shown in Fig. 8, so that the locations and structures of eddies can be easily recognized by families of closed streamlines. Note that the superflow acquires the largest velocity where the contour
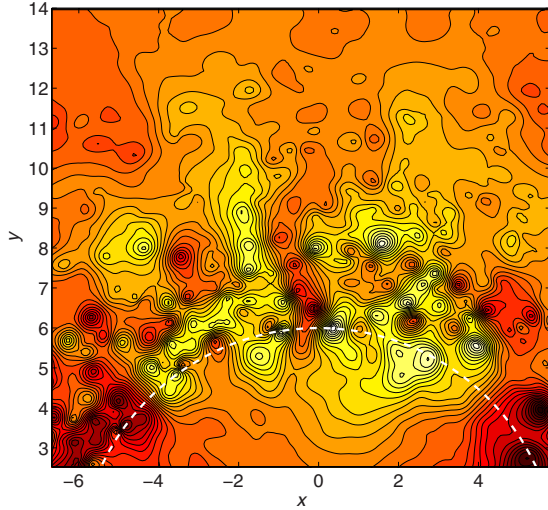
FIG. 8. (Color online) Detailed structure for part of the eddies in Fig. 7(b) are shown by the enlarged streamlines plot.

lines are closest together. Furthermore, by comparing the sizes of regions occupied by a same color [i.e., the regions characterized by the same $\phi(\boldsymbol{\rho})=C$], we conclude that the more energetic the eddy is, the larger spatial structure it possesses. Thus, considering the turbulent state represented by Fig. 2(b), the inhomogeneity of the system gives rise to a gradational spatial distribution of eddies over the area enclosing the active region of compressible field, with the largest (also the most energetic) eddies located along the border at $|\boldsymbol{\rho}|\approx 6$ and the smaller (also the less energetic) ones located more outwardly from the border.

Another subtlety yet to be addressed is the role of the compressible field in the dynamics of QT. In 2D CT, nonlinear interactions transfer energy primarily from the forcing scales to larger scales where it is ultimately dissipated by external friction while the enstrophy goes to small scales to be removed by viscosity. Recall the scaling laws in the spectrum $E_{kin}^i(k)$ and the corresponding subinertial ranges as shown in Fig. 5. In comparing our results with the cases of forcing 2D CT, we note that the transitional zone $4<k<10$ sandwiched in between the $k^{-5/3}$ and k^{-4} ranges serves as the energy input regime. This is very intriguing since there are no external forcing terms in our theoretical setting. We reason that the emergence of this energy input regime is due to the activity of sound field, as it is evident that E_{kin}^c surpasses E_{kin}^i considerably (see Fig. 5) and, above all, cannot be insulated from interchanging with the latter. Following the arguments given at the end of Sec. II, we may conceive that sound field acts as the energy source and sink simultaneously for the vortices provided that the scaling behavior of $E_{kin}^i(k)$ is held as the top concern for the current problem. Now considering that the sound waves generate vortices mostly in the outer region of BEC, we may conclude that the energy is transferred in the following two types. The first type is via the enstrophy cascade manifested by the migration of vortices toward the low-density region. This is clearly demonstrated in Fig. 4(b), where the majority of vortices generated by the input energy diffuse to the more and more dilute area and so the incompressible kinetic energy is transferred into

smaller scales. Surely, this cascading is only effective within a certain range, beyond which the density is too low to sustain the formation of vortices and, hence, the energy is eventually "dissipated" by the dilution of density. Since the total energy is conserved, the decrease in the incompressible kinetic energy is balanced by the replenishment of compressible kinetic through the sound waves emitted by the vortices when they are driven to move outwardly. This explains the emergence of Saffman's k^{-4} spectrum at large-k side despite that no authentic dissipations are introduced [25].

On the other hand, the $k^{-5/3}$ spectrum at the small-k side ($2<k<4$) demonstrates a distinct way to cascade energy. In analogy to 2D CT, we may interpret this part of spectrum as a consequence of inverse energy cascade from the forcing scales $4<k<10$ up to the larger scales with a cutoff at k_c $=2$. In 2D CT, the reciprocal of the smallest wave number specifies the size for the largest vortices available, which is normally dependent on the mechanism assumed for removing the energy. By the same token, we presume in our case that k_c^{-1} indicates a length scale comparable to the sizes of those few largest quantized vortices clumped around the rim of the condensate, where the active regions of compressible and incompressible fields overlap and the energy exchange takes place persistently and expeditiously. Considering that the overwhelming compressible field acts simultaneously as the sink and source for the incompressible field, inverse cascade occurs with energy being injected from the forcing, conveyed among the few largest vortices, and eventually dumped to the sound field all around. In fact, as the sound waves keep pulling and dragging the ambient vortices, this incoherent action prevents the accumulating of incompressible kinetic energy at large scales, so the vortices are never energetically large enough to re-enter the inner part of the condensate.

IV. CONCLUDING REMARKS

In this paper, we have investigated a 2D QT in a harmonically trapped BEC. By solving Gross-Pitaevskii equation numerically, we calculate the incompressible kinetic-energy spectrum $E_{kin}^i(k)$ for the fully turbulent superflow in the condensate. We conclude that the energy spectrum is characterized by dual cascades following the Kolmogorov-Saffman scaling laws, with $E_{kin}^i(k)\sim k^{-5/3}$ at small-k regime and $E_{kin}^i(k)\sim k^{-4}$ at large-k regime in the wave-number space.

Although our results of 2D QT in a trapped BEC possess some similarities with those of 2D CT determined by Navier-Stokes equations in classical fluid mechanics, there are some fundamental differences yet to be pointed out. First, our system described by Euler equation (after Madelung transformation) is compressible with the relationship of pressure and density being polytropic; but the Navier-Stokes equations are for incompressible flow with density being constant. Second, viscosity in Navier-Stokes equation serves as an energy sink and that means the classical fluid is a dissipative system. In BEC, there is no viscosity and, therefore, the system is nondissipative. However, the trap potential and binary interaction between particles serves as a medium for energy conversions such that the compressible and incompressible

kinetic energies can be converted into each other through this medium with compressible kinetic energy acting like sink and source for incompressible kinetic energy comparable to 2D CT. Third, our Euler equation additionally has a dispersive quantum pressure term (though small), which Navier-Stokes equations do not have. Finally, for incompressible and inviscid flow in classical fluid mechanics, a pair of point vortices with same circulation but in opposite signs are impossible to annihilate each other due to Kelvin's theorem. However, it is possible in BEC when this kind of vortices bump into each other. This is probably because the rotational incompressible kinetic energy can be almost totally turned to compressible but irrotational kinetic one.

We have verified in the present investigation that the scaling behavior of the spectrum is independent of the trapping geometry. To see whether the Kolmogorov-Saffman scaling laws are universal for all cases of 2D QT with trapped BEC, it is desirable to study the dynamics of turbulent superflows for various condensate systems, such as the dipolar BEC, two-component BEC, spinor BEC, and so forth. Results of these studies will be reported elsewhere in the near future.

[1] R. J. Donnelly, *Quantized Vortices in Helium II* (Cambridge University Press, Cambridge, 1991).

[2] R. P. Feynman, *Progress in Low Temperature Physics*, edited by C. J. Gorter (North-Holland, Amsterdam, 1955).

[3] W. F. Vinen, Proc. R. Soc. London, Ser. A **240**, 114 (1957); **240**, 128 (1957); **242**, 493 (1957).

[4] J. Maurer and P. Tabeling, Europhys. Lett. **43**, 29 (1998).

[5] S. R. Stalp, L. Skrbek, and R. J. Donnelly, Phys. Rev. Lett. **82**, 4831 (1999).

[6] T. Araki, M. Tsubota, and S. K. Nemirovskii, Phys. Rev. Lett. **89**, 145301 (2002).

[7] C. Nore, M. Abid, and M. E. Brachet, Phys. Rev. Lett. **78**, 3896 (1997); Phys. Fluids **9**, 2644 (1997).

[8] M. Kobayashi and M. Tsubota, Phys. Rev. Lett. **94**, 065302 (2005).

[9] U. Frish, *Turbulence: The Legacy of A. N. Kolmogorov* (Cambridge University Press, Cambridge, 1995).

[10] L. Pitaevskii and S. Stringari, *Bose-Einstien Condensation* (Oxford University Press, Oxford, 2003).

[11] C. Lobo, A. Sinatra, and Y. Castin, Phys. Rev. Lett. **92**, 020403 (2004).

[12] N. G. Parker and C. S. Adams, Phys. Rev. Lett. **95**, 145301 (2005).

[13] A. A. Norrie, R. J. Ballagh, and C. W. Gardiner, Phys. Rev. Lett. **94**, 040401 (2005).

[14] M. Kobayashi and M. Tsubota, Phys. Rev. A **76**, 045603 (2007).

[15] T.-L. Horng, C.-H. Hsueh, and S.-C. Gou, Phys. Rev. A **77**, 063625 (2008); T.-L. Horng, S.-C. Gou, and T.-C. Lin, *ibid.* **74**, 041603(R) (2006).

[16] E. J. M. Madarassy and C. F. Barenghi, Geophys. Astrophys. Fluid Dyn. **103**, 269 (2009).

[17] R. H. Kraichnan, Phys. Fluids **10**, 1417 (1967).

[18] G. K. Batchelor, Phys. Fluids Suppl. II **12**, 233 (1969).

[19] *Mathematical and Physical Theory of Turbulence*, edited by J. Cannon and B. Shivamoggi (Chapman & Hall/CRC, Boca Raton, FL, 2006).

[20] C.-S. Hsueh, S.-C. Gou, T.-L. Horng, and Y.-M. Kao, J. Phys. B **40**, 4561 (2007).

[21] L. V. Hau, Nat. Phys. **3**, 13 (2007).

[22] P. G. Saffman, Stud. Appl. Math. **L**, 377 (1971).

[23] M. Kobayashi and M. Tsubota, J. Phys. Soc. Jpn. **74**, 3248 (2005).

[24] J. S. Marshall, *Inviscid Incompressible Flow* (John Wiley & Sons, New York, 2001).

[25] C. F. Barenghi, N. G. Parker, N. P. Proukakis, and C. S. Adams, J. Low Temp. Phys. **138**, 629 (2005).